Natural Resources for Human Health
eISSN: 2583-1194

Original Research

Received 18 March 2026
Revised 20 April 2026
Accepted 16 May 2026

Natural Resources for Human Health 2026, Vol. 6 (1s): 401–418

KEYWORDS:
Neutrophil extracellular traps; NETosis; rheumatoid arthritis; collagen-induced arthritis; Myricetin; PAD4 inhibition; citrullinated histone H3; ACPA; MPO-DNA; CI-Amidine

NETosis-Associated Biomarkers and Pro-Inflammatory Cytokines in Collagen-Induced Arthritis: Therapeutic Modulation by Myricetin, RL6 (1,8-Naphthalimide), and CI-Amidine in an Albino Mouse Model

Ahmed Shandookh Hameed[1], Wafaa Sadoon Shani[2]

[1,2] Biology Department, College of Science, Basrah University. Iraq
[1] ahmedalsaidi@stu.edu.iq
[2] wafaa_sadoon@yahoo.com
*Corresponding Author Email: ahmedalsaidi@stu.edu.iq

ABSTRACT:

Background: Neutrophil extracellular trap (NET) formation — NETosis — plays a central role in rheumatoid arthritis (RA) pathogenesis by generating citrullinated autoantigens that drive autoimmunity and perpetuating synovial inflammation through pro-inflammatory cytokine release. Despite growing evidence, integrated therapeutic targeting of the NET-cytokine-autoantibody axis remains incompletely explored.

Objectives: This study investigated NETosis-associated biomarkers and inflammatory mediators in a collagen-induced arthritis (CIA) mouse model and evaluated the therapeutic efficacy of three mechanistically distinct agents: Myricetin (natural flavonol; MPO and PADI4 inhibitor), RL6 (1,8-Naphthalimide; MPO inhibitor), and CI-Amidine (selective PAD4 inhibitor).

Methods: One hundred and eighty male albino mice were allocated into six groups (n=30 per group): negative control (G1), CIA-induced (G2), CIA untreated chronic (G3), CIA + Myricetin (G4), CIA + RL6 (G5), and CIA + CI-Amidine (G6). Seven biomarkers were quantified by ELISA: MPO-DNA, NE-DNA, IL-6, IL-1β, TNF-α, Cit H3-NE, and ACPA. NET formation was confirmed by fluorescence microscopy. One-way ANOVA with Games-Howell post-hoc test was applied.

Results: CIA induction produced dramatic elevations across all biomarkers, with Cit H3-NE showing the most striking increase (23.96-fold above control; $P<0.0001$). Progressive ACPA elevation from G2 (74.57±19.60 ng/mL) to G3 (81.87±6.17 ng/mL) demonstrated the self-amplifying autoimmune loop. All three therapeutic agents completely normalized Cit H3-NE to control levels. Myricetin demonstrated superior cytokine suppression (88.4% TNF-α reduction). Pearson correlation revealed the strongest IL-6–ACPA association in chronic CIA ($r=0.74$, $P<0.001$).

Conclusion: This study provides comprehensive evidence that NETosis drives RA pathogenesis through an integrated NET-cytokine-autoantibody axis. Myricetin, RL6, and CI-Amidine demonstrated significant anti-NETotic efficacy through distinct but convergent mechanisms, positioning NETosis as a viable multi-target therapeutic strategy in RA.

1. INTRODUCTION

Rheumatoid arthritis (RA) is a persistent autoimmune inflammatory disorder that predominantly affects the synovial joints, causing symmetrical inflammation presenting as morning stiffness lasting more than one hour, pain, swelling, deformity, and progressive loss of mobility. The primary pathological site in RA is the synovial tissue, which undergoes hyperplastic transformation into a pathologically invasive tissue called pannus, consisting of activated immune cells and fibroblast-like synoviocytes (FLSs) capable of invading adjacent cartilage and bone, resulting in chronic and irreversible joint destruction (McInnes & Schett, 2011; Smolen et al., 2016; Coutant & Miossec, 2020). The processes involved in RA development are multifactorial, encompassing genetic predisposition linked to HLA-DRB1 shared epitope alleles, environmental triggers including tobacco smoke and viral/bacterial infections, and dysregulation of both innate and adaptive immune systems (Kurko et al., 2013; Makrygiannakis et al., 2008; Chen et al., 2013; Sparks, 2019).

A hallmark of RA pathogenesis is the generation of anti-citrullinated protein antibodies (ACPAs), which are highly specific for RA and detectable years before clinical onset. ACPAs arise through citrullination — the post-translational conversion of peptidyl arginine to citrulline via peptidyl arginine deiminase (PAD) enzymes — generating neoantigens that trigger autoimmune responses (Nielen et al., 2004; Liu et al., 2022; van Delft & Huizinga, 2020; Spengler et al., 2015). Pro-inflammatory cytokines, particularly TNF-α, IL-6, and IL-1β, drive synovial inflammation, osteoclast differentiation, and cartilage degeneration in a self-sustaining inflammatory loop (McInnes & Schett, 2011; Smolen et al., 2016; Wright et al., 2020).Neutrophils represent the most abundant leukocytes in the synovial fluid of RA patients and have emerged as critical drivers of disease pathogenesis. In RA, neutrophils are characterized by delayed apoptosis, increased ROS production, and enhanced release of myeloperoxidase (MPO) and neutrophil elastase (NE) (Wright et al., 2014; O'Neil & Kaplan, 2019; Denny et al., 2010). A particularly pro-inflammatory subset, low-density neutrophils (LDNs), generates neutrophil extracellular traps (NETs) to a greater extent than conventional neutrophils, with their abundance correlating with disease severity (Wright et al., 2017). NETs are extracellular structures produced when neutrophils undergo NETosis, expelling decondensed chromatin decorated with MPO, NE, and citrullinated histone H3 (CitH3) into the extracellular space (Brinkmann et al., 2004; Papayannopoulos, 2018). NETosis occurs via suicidal NETosis (NADPH oxidase-dependent) and vital NETosis (without cell death) (Thiam et al., 2020; Metzler et al., 2011).

In RA, NETs serve as a critical source of citrullinated autoantigens — including modified histones and vimentin — stimulating ACPA production and perpetuating autoimmune responses (Khandpur et al., 2013; Corsiero et al., 2016; Chowdhury et al., 2014; Wang et al., 2018). NET components activate macrophages, dendritic cells, and T cells, driving TNF-α, IL-6, and IL-1β production, creating an intrinsic feedback loop perpetuating chronic synovial destruction (Carmona-Rivera et al., 2017; Chatfield et al., 2022; Apel et al., 2023).

Three mechanistically distinct anti-NETotic agents were investigated: CI-Amidine, a selective PAD4 inhibitor preventing histone citrullination and NET formation (Fousert et al., 2020; Zhao et al., 2021); RL6 (1,8-Naphthalimide), an MPO inhibitor suppressing oxidative burst-driven NET release (Wang et al., 2023); and Myricetin, a natural flavonol that inhibits NETosis through direct binding to both MPO and PADI4, preventing their nuclear translocation and reducing CitH3 expression (Shu et al., 2024; Lee & Choi, 2010; Jose et al., 2024). This study aimed to comprehensively investigate the NET-cytokine-autoantibody axis in CIA and evaluate the integrated therapeutic efficacy of these three agents.

2. MATERIALS AND METHODS

2.1 Ethical Approval

All experimental procedures were conducted in strict accordance with institutional animal ethics guidelines. All efforts were made to minimize animal suffering, in compliance with the 3Rs principles (Replacement, Reduction, and Refinement).

2.2 Experimental Animals

One hundred and eighty male albino mice, aged 8–10 weeks and weighing 25–40 g, were obtained from a certified animal facility and housed under standardized conditions: 12-hour light/dark cycle, temperature 22 ± 2°C, humidity 55 ± 5%, ad libitum food and water. Animals were acclimatized for one week prior to experiments.

2.3 Experimental Groups

Animals were randomly allocated into six groups (n=30 per group):

Table 1. Experimental groups and treatment protocols.

Group	Designation	n	Description
G1	Negative Control	30	Healthy albino mice; no CIA induction. Baseline reference for all biomarkers.
G2	RA-Induced (CIA)	30	CIA-induced mice sacrificed at day 28 (peak acute inflammation phase).
G3	RA Untreated (+)	30	CIA-induced mice with no treatment; sacrificed at day 49 (chronic disease phase).
G4	RA + Myricetin	30	CIA mice treated with Myricetin (MPO + PADI4 inhibitor) from day 28–49.
G5	RA + RL6	30	CIA mice treated with RL6 / 1,8-Naphthalimide (MPO inhibitor) from day 28–49.
G6	RA + CI-Amidine	30	CIA mice treated with CI-Amidine (selective PAD4 inhibitor) from day 28–49.

Note: *CIA: Collagen-Induced Arthritis; PAD4: Peptidyl Arginine Deiminase 4; MPO: Myeloperoxidase.*

2.4 CIA Induction Protocol

Collagen-induced arthritis was established using a two-component simultaneous injection protocol. On Day 0, each mouse received: (1) an intra-articular injection of 10 µL of type II collagen (CII) solution (dissolved in 0.1 M acetic acid at 2 mg/mL) directly into the right knee joint using a 29-gauge needle under brief isoflurane anesthesia; and (2) a subcutaneous injection of 100 µL of complete Freund's adjuvant (CFA) supplemented with Mycobacterium tuberculosis H37Ra (4 mg/mL) at the base of the tail to stimulate systemic immune activation. A booster dose was administered on Day 14 following the identical protocol (10 µL intra-articular CII + 100 µL subcutaneous CFA). Disease severity was monitored using a standardized arthritis scoring system (0–4 per paw, maximum 16) every three days from Day 7 onwards.

2.5 Therapeutic Agents

Myricetin (≥98% purity; Sigma-Aldrich) was administered orally at 5 mg/kg/day dissolved in 0.5% carboxymethylcellulose. RL6 (1,8-Naphthalimide; ≥97% purity; Sigma-Aldrich) was administered intraperitoneally at the established therapeutic dose. CI-Amidine (≥98% purity; Cayman Chemical) was administered intraperitoneally at 10 mg/kg three times weekly, consistent with published PAD4 inhibitor protocols (Fousert et al., 2020; Zhao et al., 2021). All treatments were administered from day 28 to day 49.

2.6 Sample Collection

Animals were anesthetized with ketamine/xylazine (80/10 mg/kg) at sacrifice. Blood was collected via cardiac puncture, allowed to clot at room temperature, and serum separated by centrifugation (3,000 rpm, 15 minutes, 4°C). Samples were stored at −80°C until analysis.

2.7 ELISA Quantification

Table 2. Commercial ELISA kits used for biomarker quantification.

Biomarker	Kit Name	Manufacturer	Cat. No.
MPO-DNA Complex	Mouse MPO-DNA ELISA Kit	SinoGeneclon Co., Ltd	SG-35905
NE-DNA Complex	Mouse NE-DNA ELISA Kit	SinoGeneclon Co., Ltd	SG-35904
IL-6	Mouse IL-6 ELISA Kit	FineTest/Roedemesis	RDEEM0121

IL-1β	Mouse IL-1β ELISA Kit	FineTest/Roedemesis	RDEEM0109
TNF-α	Mouse TNF-α ELISA Kit	FineTest/Roedemesis	RDEEM0183
Cit H3-NE	Mouse H3cit-NE ELISA Kit	Roedemesis Medical Supply	RDEEM2516
ACPA	Mouse ACPA ELISA Kit	ELK Biotechnology	ELK0589

Note: *All ELISA kits were used according to manufacturers' protocols. Optical density measured at 450 nm. All samples run in duplicate.*

2.8 Fluorescence Microscopy

Detection of neutrophil extracellular traps (NETs) in synovial fluid was performed using a direct visualization protocol. Synovial fluid was collected from the right knee joint of experimental animals at the designated sacrifice time points by intra-articular lavage using normal saline (0.9% NaCl). Briefly, a small volume of normal saline was injected into the right knee joint cavity using a sterile syringe, followed by gentle aspiration of the lavage fluid. A small volume of the collected synovial lavage fluid was placed directly onto clean glass slides and allowed to settle for 5 minutes at room temperature. Slides were then stained with SYTOX Green nucleic acid stain (500 nM; Thermo Fisher Scientific) for 15 minutes at room temperature, protected from light. NET formation was examined directly by fluorescence microscopy at 488 nm excitation wavelength. The extent of NET formation was assessed by quantifying the percentage of cells displaying characteristic NET structures — extracellular web-like DNA morphology — across five random microscopic fields per sample."

2.9 Statistical Analysis

All analyses were performed using IBM SPSS Statistics, Version 26. Differences among groups were assessed by one-way ANOVA followed by Games-Howell post-hoc test (does not assume variance homogeneity). Pearson correlation coefficient (r) evaluated inter-biomarker relationships within each group. $P < 0.05$ was considered statistically significant. Results expressed as Mean ± SD with superscript letters (a–f) indicating statistically distinct groups.

3. RESULTS

3.1 Clinical Observations

G1 (Negative Control) mice displayed normal posture, symmetrical limb morphology, and no arthritic signs throughout the experimental period (Figure 1A). G2 (RA-Induced) mice developed visible polyarthritis by day 14–21, including marked paw swelling, erythema, digital deformity, and loss of normal limb posture (Figure 1B), confirming successful CIA establishment.

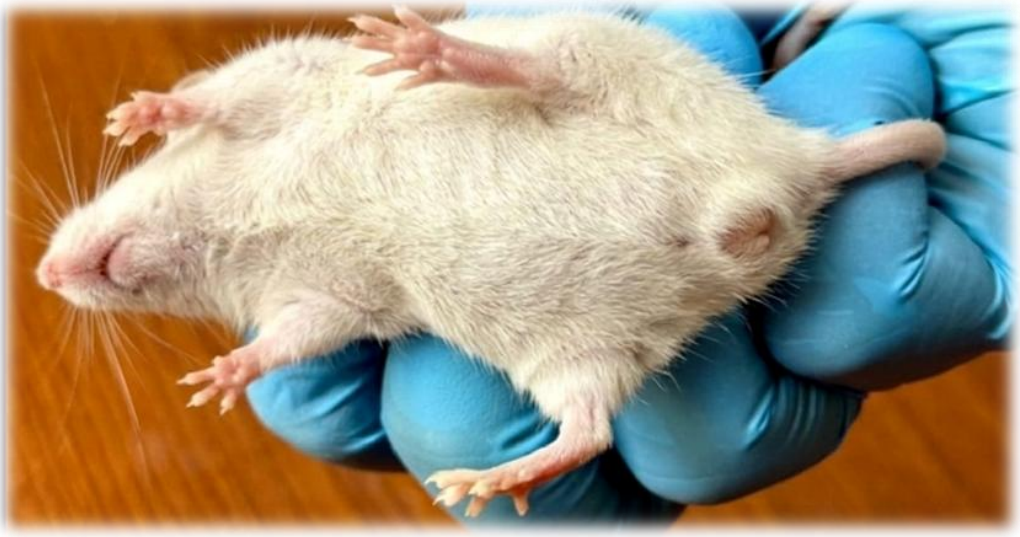

Figure 1. Representative photographs of experimental animals. (A) Healthy albino mouse from G1 (Negative Control) showing normal posture and no arthritic signs

Figure 2. Representative photographs of experimental animals. (B) CIA-induced mouse from G2 (RA-Induced) demonstrating marked polyarthritis: paw swelling, erythema, and digital deformity confirming successful CIA induction.

3.2 Serum MPO-DNA Complex Levels

MPO-DNA levels demonstrated highly significant inter-group differences (one-way ANOVA, P<0.0001). G2 recorded the highest concentration (373.32±59.23 ng/mL), a 21.3-fold elevation above G1 (17.50±3.75 ng/mL). G3 remained markedly elevated (227.58±54.64 ng/mL). Among treatment groups, G4 achieved the greatest reduction (43.87±7.84 ng/mL, letter d). G5 and G6 showed statistically equivalent reductions (59.18±9.13 and 57.47±10.34 ng/mL, both letter c).

Table 3. Serum MPO-DNA Complex (ng/mL) levels among the experimental groups.

Group	Mean ± SD (ng/mL)	Significance	P-value
G1: Negative Control	17.50±3.75	f	<0.0001***
G2: RA-Induced (CIA)	373.32±59.23	a	
G3: RA Untreated (+)	227.58±54.64	b	
G4: RA + Myricetin	43.87±7.84	d	
G5: RA + RL6	59.18±9.13	c	
G6: RA + CI-Amidine	57.47±10.34	c	

Note: *Values are Mean ± SD (n=30 per group). Superscript letters (a–f) indicate statistically distinct groups by one-way ANOVA followed by Games-Howell post-hoc test (P<0.0001). Groups sharing the same letter are not significantly different.*

3.3 Serum NE-DNA Complex Levels

G2 exhibited the highest NE-DNA (145.60±19.71 ng/mL), a 16.7-fold elevation above G1 (8.70±2.45 ng/mL). G3 remained elevated (73.89±10.86 ng/mL). G6 achieved the greatest reduction (53.40±9.97 ng/mL, letter d), G4 showed comparable efficacy (55.14±9.57 ng/mL, letter cd), and G5 demonstrated intermediate reduction (66.89±20.52 ng/mL, letter bc).

Table 4. Serum NE-DNA Complex (ng/mL) levels among the experimental groups.

Group	Mean ± SD (ng/mL)	Significance	P-value
G1: Negative Control	8.70±2.45	e	
G2: RA-Induced (CIA)	145.60±19.71	a	

G3: RA Untreated (+)	73.89±10.86	b	<0.0001***
G4: RA + Myricetin	55.14±9.57	cd	
G5: RA + RL6	66.89±20.52	bc	
G6: RA + CI-Amidine	53.40±9.97	d	

Note: *Values are Mean ± SD (n=30 per group). Superscript letters (a–f) indicate statistically distinct groups by one-way ANOVA followed by Games-Howell post-hoc test (P<0.0001). Groups sharing the same letter are not significantly different.*

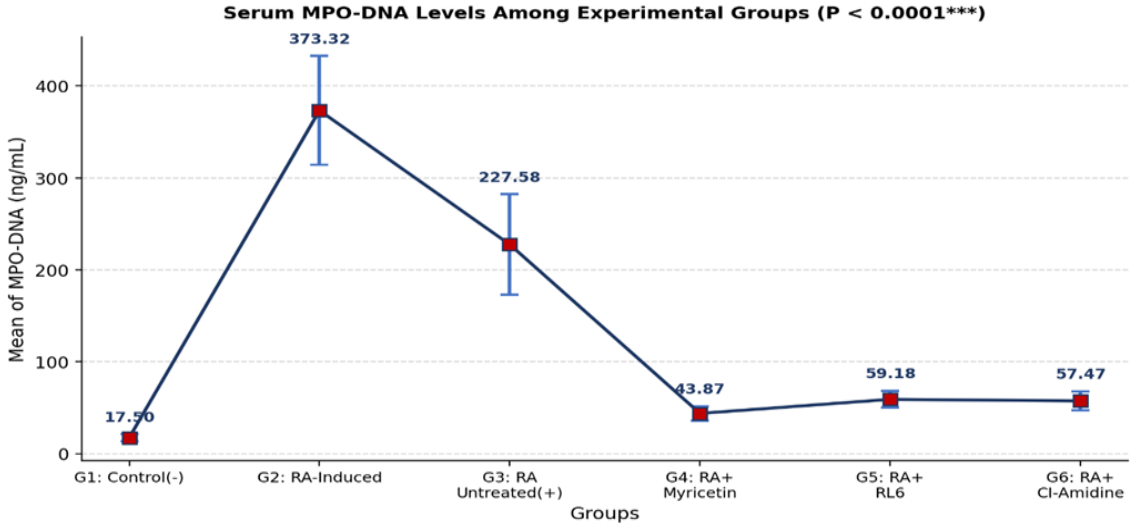

Figure 3. Serum NE-DNA Complex levels (ng/mL) among experimental groups. Values are Mean ± SD (n=30 per group). P<0.0001***.

3.4 Serum IL-6 Levels

G3 (79.12±7.88 pg/mL) marginally exceeded G2 (74.04±14.85 pg/mL), both sharing letter a, reflecting the self-amplifying IL-6 loop in chronic CIA. G4 achieved the greatest reduction (36.70±3.71 pg/mL, letter e — 53.6% vs G3). G6 reduced IL-6 to 45.96±5.33 pg/mL (letter d). G5 showed 57.91±16.01 pg/mL (letter c).

Table 5. Serum IL-6 (pg/mL) levels among the experimental groups.

Group	Mean ± SD (pg/mL)	Significance	P-value
G1: Negative Control	1.97±0.45	f	<0.0001***
G2: RA-Induced (CIA)	74.04±14.85	a	
G3: RA Untreated (+)	79.12±7.88	a	
G4: RA + Myricetin	36.70±3.71	e	
G5: RA + RL6	57.91±16.01	c	
G6: RA + CI-Amidine	45.96±5.33	d	

Note: *Values are Mean ± SD (n=30 per group). Superscript letters (a–f) indicate statistically distinct groups by one-way ANOVA followed by Games-Howell post-hoc test (P<0.0001). Groups sharing the same letter are not significantly different.*

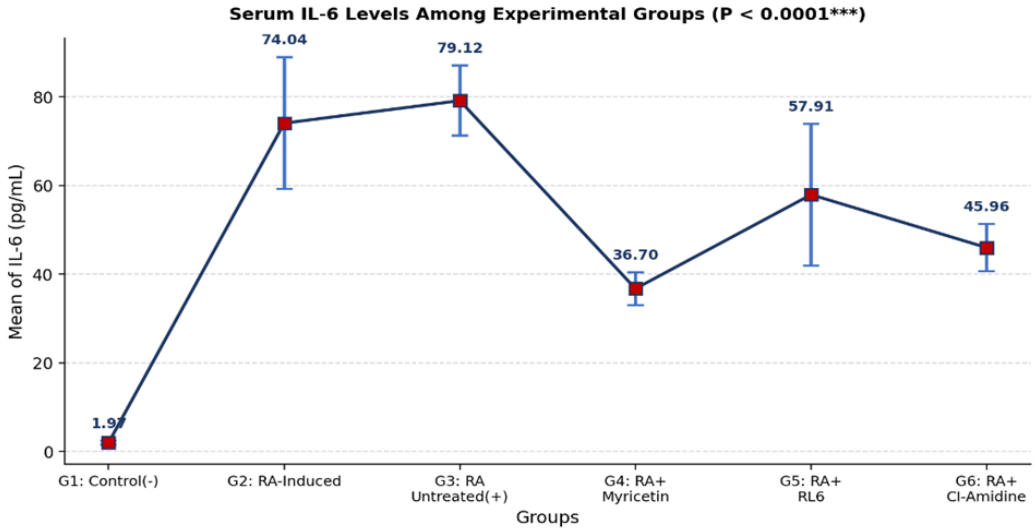

Figure 4. *Serum IL-6 levels (pg/mL) among experimental groups. Values are Mean ± SD (n=30 per group). P<0.0001***.*

3.5 Serum IL-1β Levels

G2 (84.58±27.12 pg/mL) and G3 (84.15±14.08 pg/mL) showed equivalent IL-1β elevation (letter a), confirming sustained NLRP3 inflammasome activation. G5 demonstrated the least suppression (75.82±11.65 pg/mL, letter ab). G6 (53.20±9.90, letter cd) and G4 (59.00±8.92, letter c) achieved greater suppression.

Table 6. Serum IL-1β (pg/mL) levels among the experimental groups.

Group	Mean ± SD (pg/mL)	Significance	P-value
G1: Negative Control	29.45±8.13	e	<0.0001***
G2: RA-Induced (CIA)	84.58±27.12	a	
G3: RA Untreated (+)	84.15±14.08	a	
G4: RA + Myricetin	59.00±8.92	c	
G5: RA + RL6	75.82±11.65	ab	
G6: RA + CI-Amidine	53.20±9.90	cd	

Note: *Values are Mean ± SD (n=30 per group). Superscript letters (a–f) indicate statistically distinct groups by one-way ANOVA followed by Games-Howell post-hoc test (P<0.0001). Groups sharing the same letter are not significantly different.*

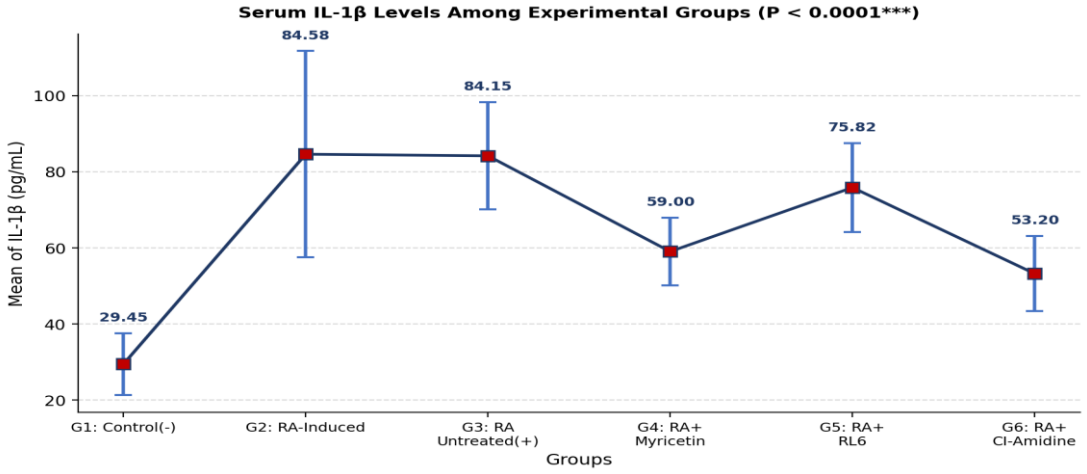

Figure 5. Serum IL-1β levels (pg/mL) among experimental groups. Values are Mean ± SD (n=30 per group). P<0.0001***.

3.6 Serum TNF-α Levels

G2 (225.19±13.51 pg/mL) and G3 (217.99±13.99 pg/mL) were statistically equivalent (letter a). G4 achieved a remarkable 88.4% TNF-α reduction (26.11±5.66 pg/mL, letter d), approaching control levels. G5 and G6 showed equivalent reductions (64.71±15.87 and 64.58±14.16 pg/mL, letter c).

Table 7. Serum TNF-α (pg/mL) levels among the experimental groups.

Group	Mean ± SD (pg/mL)	Significance	P-value
G1: Negative Control	6.99±3.46	e	<0.0001***
G2: RA-Induced (CIA)	225.19±13.51	a	
G3: RA Untreated (+)	217.99±13.99	a	
G4: RA + Myricetin	26.11±5.66	d	
G5: RA + RL6	64.71±15.87	c	
G6: RA + CI-Amidine	64.58±14.16	c	

Note: *Values are Mean ± SD (n=30 per group). Superscript letters (a–f) indicate statistically distinct groups by one-way ANOVA followed by Games-Howell post-hoc test (P<0.0001). Groups sharing the same letter are not significantly different.*

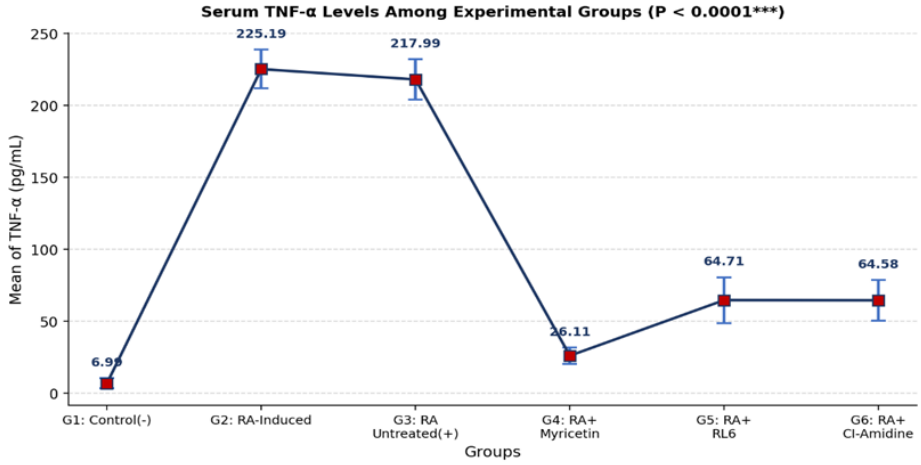

Figure 6. Serum TNF-α levels (pg/mL) among experimental groups. Values are Mean ± SD (n=30 per group). P<0.0001***.

3.7 Serum Cit H3-NE Complex Levels

G2 recorded the highest Cit H3-NE (26.84±8.80 ng/mL), a 23.96-fold elevation above G1 (1.12±0.54 ng/mL). G3 remained elevated (21.54±2.32 ng/mL, letter b). The most critical finding: all three treatment groups completely normalized Cit H3-NE to control levels (letter c): G4=1.07±0.67, G5=1.85±0.70, G6=1.17±0.54 ng/mL, constituting the strongest evidence of NETosis abolition in this study.

Table 8. Serum Cit H3-NE Complex (ng/mL) levels among the experimental groups.

Group	Mean ± SD (ng/mL)	Significance	P-value
G1: Negative Control	1.12±0.54	c	<0.0001***
G2: RA-Induced (CIA)	26.84±8.80	a	
G3: RA Untreated (+)	21.54±2.32	b	
G4: RA + Myricetin	1.07±0.67	c	
G5: RA + RL6	1.85±0.70	c	
G6: RA + CI-Amidine	1.17±0.54	c	

Note: *Values are Mean ± SD (n=30 per group). Superscript letters (a–f) indicate statistically distinct groups by one-way ANOVA followed by Games-Howell post-hoc test (P<0.0001). Groups sharing the same letter are not significantly different.*

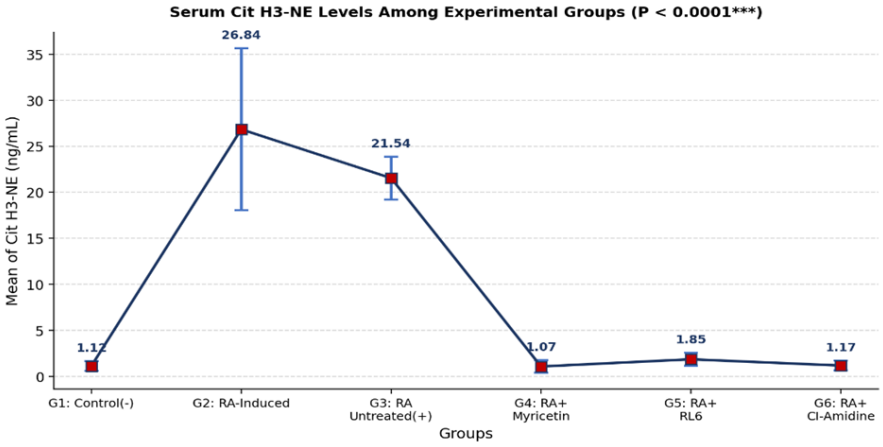

Figure 7. Serum Cit H3-NE Complex levels (ng/mL) among experimental groups. Values are Mean ± SD (n=30 per group). P<0.0001***.

3.8 Serum ACPA Levels

G3 exhibited the highest ACPA (81.87±6.17 ng/mL, letter a), exceeding G2 (74.57±19.60 ng/mL, letter b), reflecting ACPA amplification in chronic CIA. G6 (40.52±7.64, letter c) and G4 (44.56±4.85, letter c) showed equivalent suppression reflecting their shared PAD4-inhibitory capacity. G5 demonstrated intermediate reduction (51.28±6.13 ng/mL, letter d).

Table 9. Serum ACPA (ng/mL) levels among the experimental groups.

Group	Mean ± SD (ng/mL)	Significance	P-value
G1: Negative Control	6.69±3.32	e	<0.0001***
G2: RA-Induced (CIA)	74.57±19.60	b	
G3: RA Untreated (+)	81.87±6.17	a	
G4: RA + Myricetin	44.56±4.85	c	
G5: RA + RL6	51.28±6.13	d	
G6: RA + CI-Amidine	40.52±7.64	c	

Note: *Values are Mean ± SD (n=30 per group). Superscript letters (a–f) indicate statistically distinct groups by one-way ANOVA followed by Games-Howell post-hoc test (P<0.0001). Groups sharing the same letter are not significantly different.*

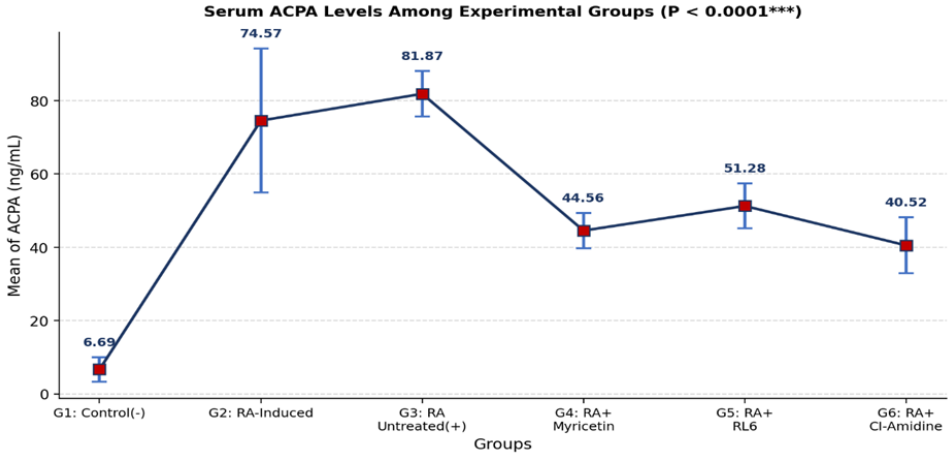

Figure 8. Serum ACPA levels (ng/mL) among experimental groups. Values are Mean ± SD (n=30 per group). P<0.0001***.

3.9 Pearson Correlation Analysis

In G1, no significant correlations were detected, confirming absence of inflammatory network activation under physiological conditions. In G2, a highly integrated network emerged, with the strongest associations between NE–Cit H3 (r=0.69, P<0.001), MPO–IL-6 (r=0.66, P<0.001), and Cit H3–ACPA (r=0.66, P<0.001). In G3, the strongest correlation in the entire study was IL-6–ACPA (r=0.74, P<0.001). In G4, the NE–Cit H3 correlation was attenuated to r=0.42 (P=0.021). In G5, retained MPO–NE (r=0.53) and MPO–ACPA (r=0.51) correlations indicate persistent granule coupling. In G6, the strongest association was Cit H3–ACPA (r=0.59, P=0.001).

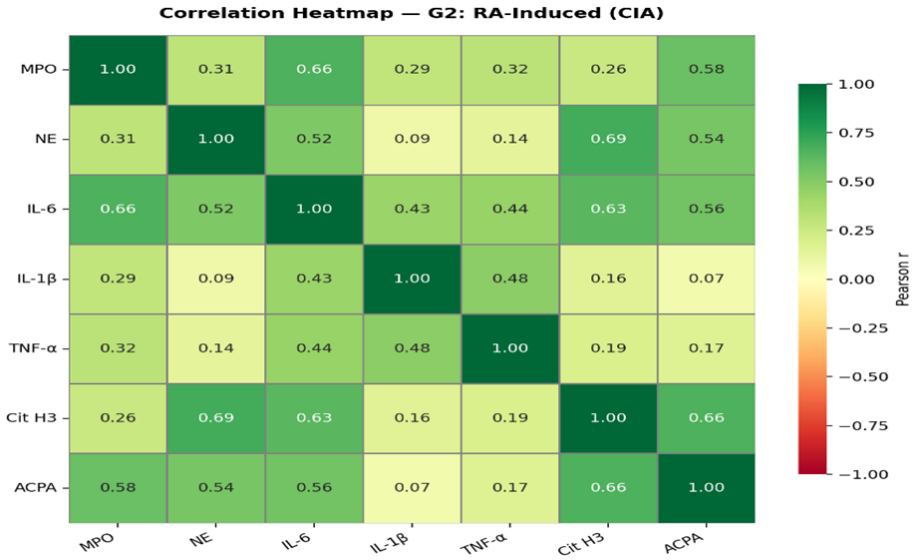

Figure 9. Correlation heatmap — G1 (Negative Control). No significant correlations detected. Green=positive, red/yellow=negative. Values are Pearson r. *P<0.05, **P<0.01.

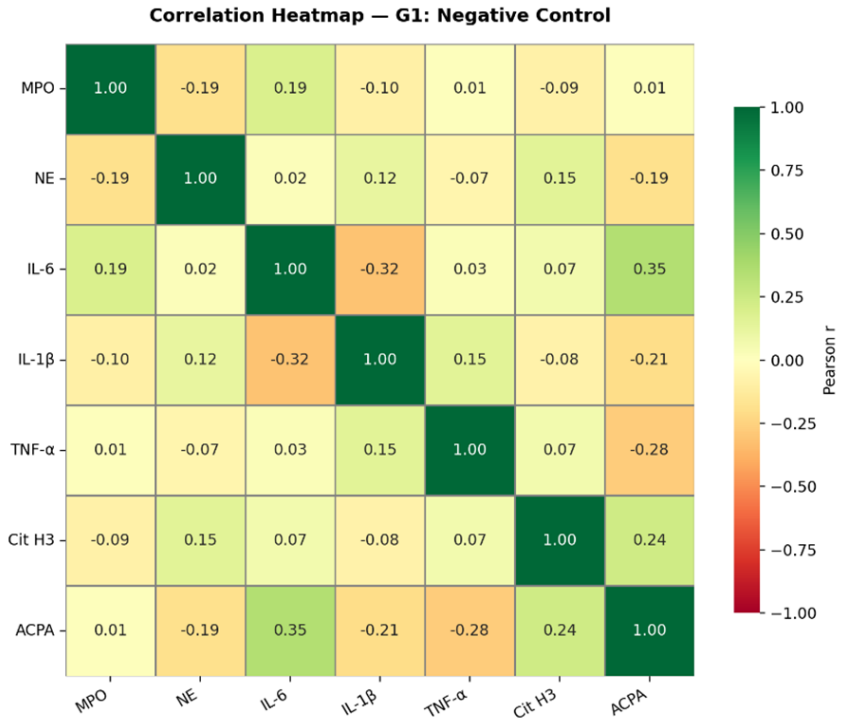

Figure 10. Correlation heatmap — G2 (RA-Induced CIA). Dense positive network reflecting active NETosis. Strongest: NE–Cit H3 (r=0.69**), MPO–IL-6 (r=0.66**), Cit H3–ACPA (r=0.66**).

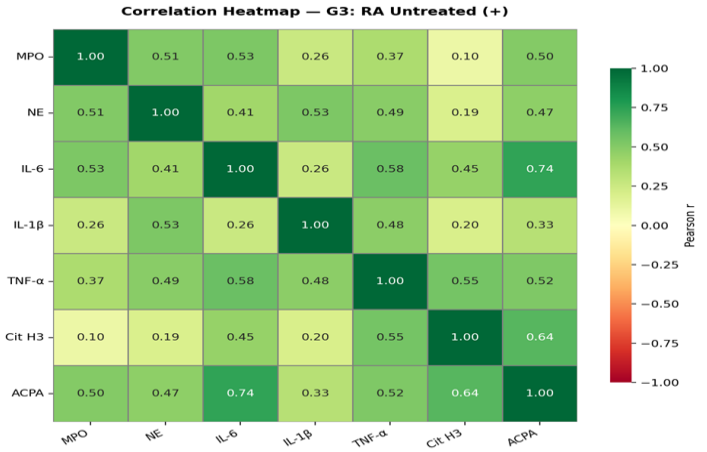

Figure 11. Correlation heatmap — G3 (RA Untreated). Expanded network with strongest study correlation IL-6–ACPA (r=0.74**), reflecting chronic autoimmune loop entrenchment.

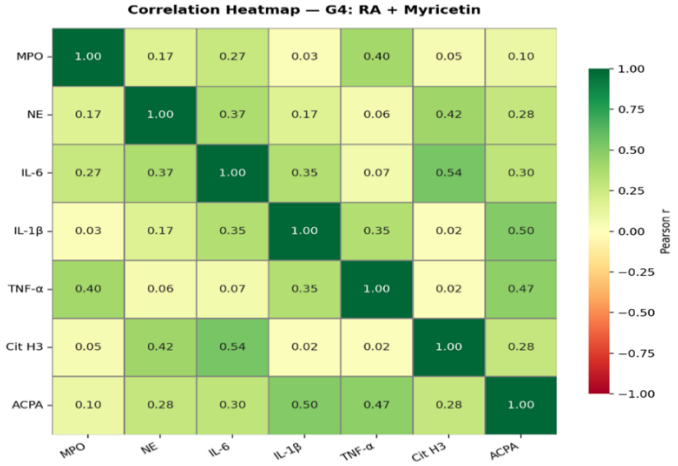

Figure 12. Correlation heatmap — G4 (RA + Myricetin). Substantially disrupted network. NE–Cit H3 attenuated to r=0.42*, consistent with dual MPO/PADI4 inhibition.

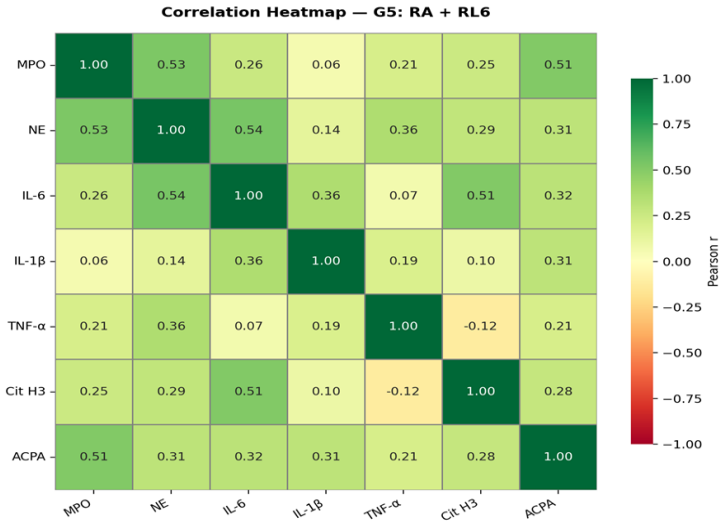

Figure 13. Correlation heatmap — G5 (RA + RL6). Retained MPO–NE (r=0.53**) and NE–IL-6 (r=0.54**) reflecting selective MPO inhibition pattern.

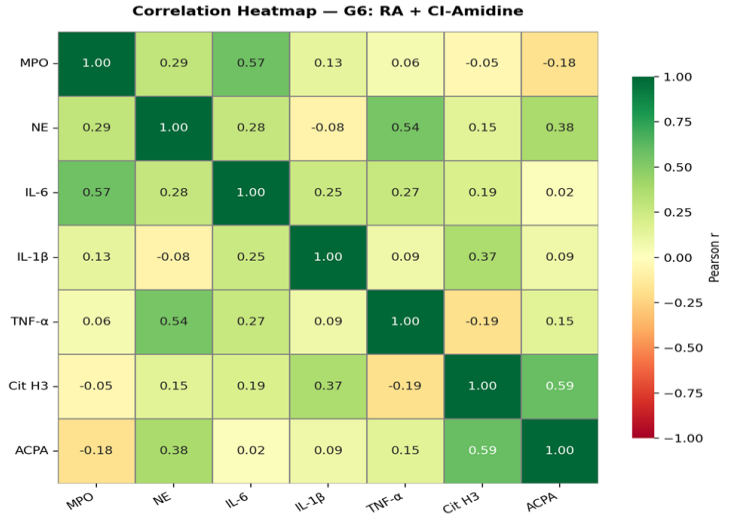

Figure 14. Correlation heatmap — G6 (RA + CI-Amidine). Strongest: Cit H3–ACPA (r=0.59**), suggesting residual citrullinated antigen generation despite PAD4 inhibition.

3.10 Fluorescence Microscopy Detection of NETs

SYTOX Green fluorescence microscopy provided direct visual evidence of NETosis. G2 neutrophils demonstrated intense NET formation with dense extracellular DNA (Figure 15). G3 showed persistent scattered NET release (Figure 16). High-magnification imaging revealed individual neutrophils with well-defined NET structures with extending fibers (Figure 17). Treatment groups (G4–G6) demonstrated markedly reduced fluorescence, confirming near-complete NETosis suppression (Figure 18).

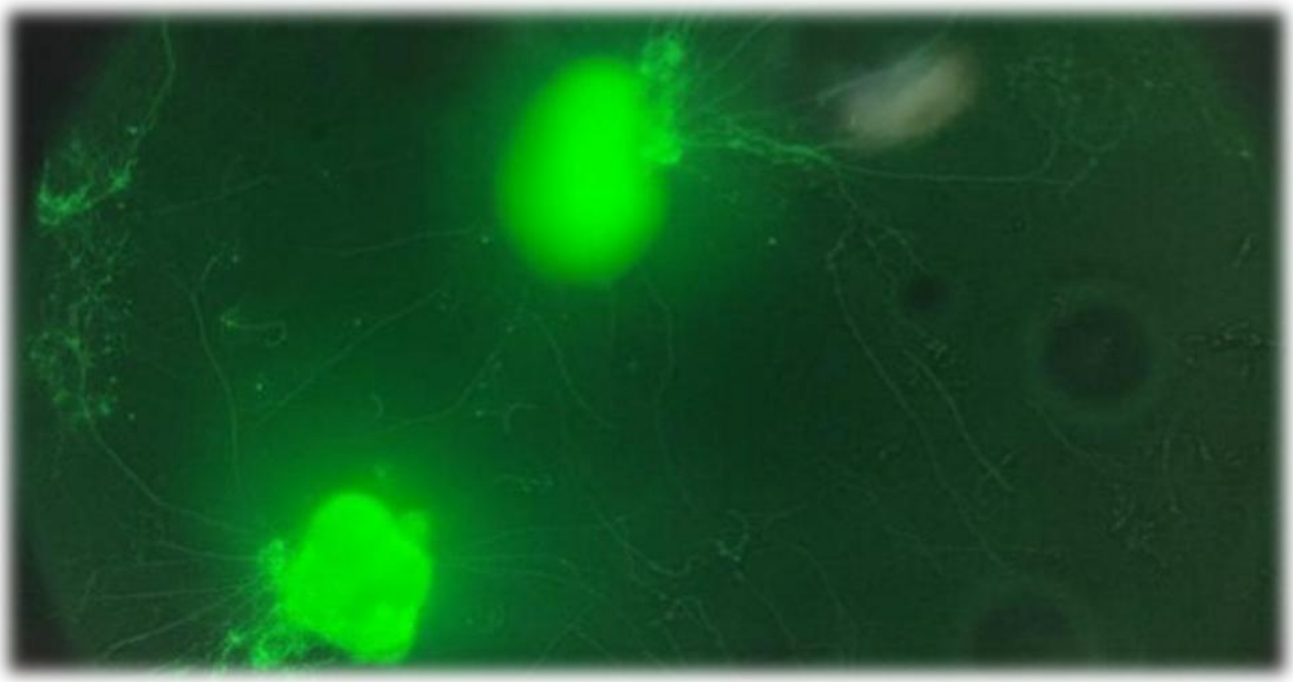

Figure 15. Synovial lavage fluid from G2 (RA-Induced CIA). Advanced NETosis showing dense extracellular chromatin release with characteristic web-like DNA structures, indicative of active neutrophil extracellular trap formation at peak CIA. SYTOX Green staining.

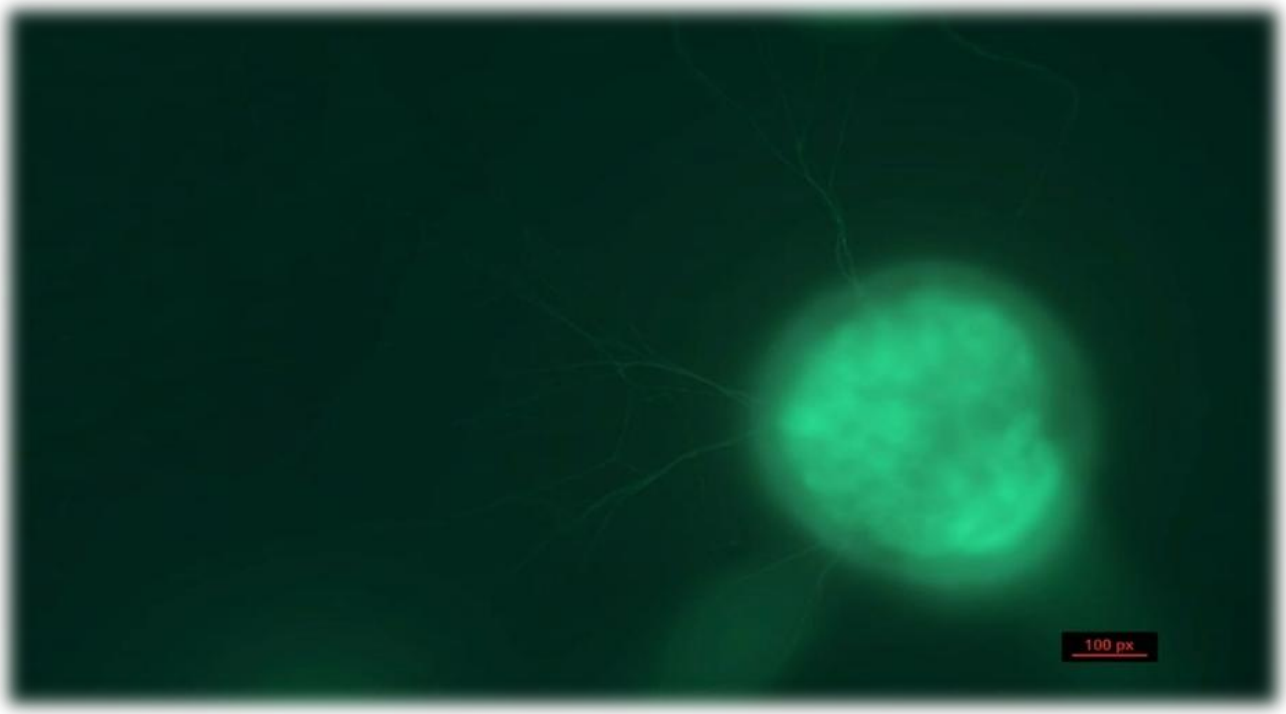

Figure 16. Synovial lavage fluid from treatment groups (G4–G6). Markedly reduced extracellular DNA release with minimal chromatin decondensation, confirming near-complete suppression of NETosis following therapeutic intervention with Myricetin, RL6, and CI-Amidine. SYTOX Green staining. Scale bar = 100 μm

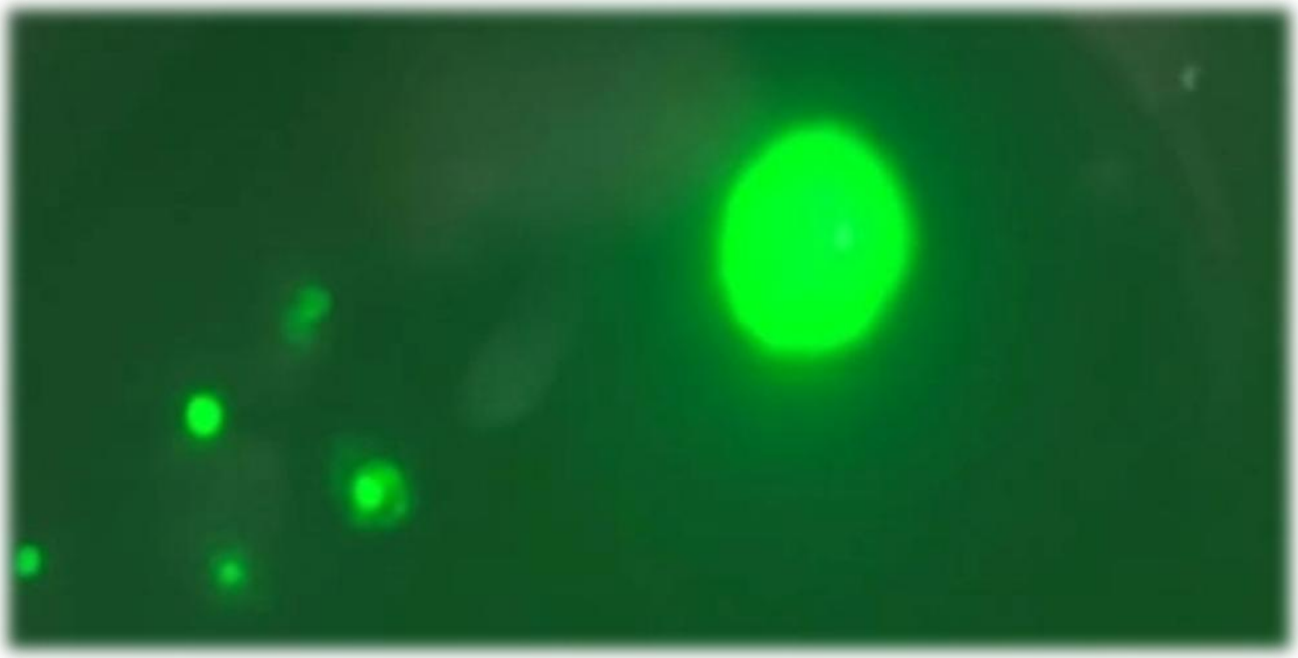

Figure 17. Synovial lavage fluid from G1 (Negative Control). Intact neutrophil with fully condensed chromatin and no extracellular DNA release, confirming the complete absence of NETosis under normal physiological conditions. SYTOX Green staining.

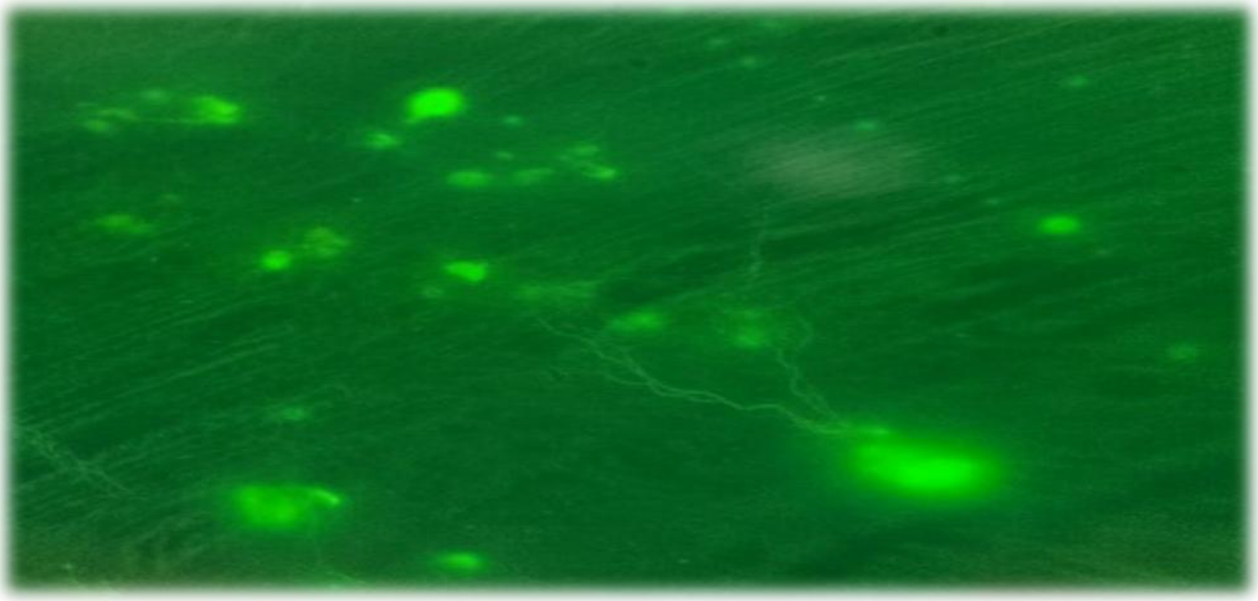

Figure 18. Synovial lavage fluid from G3 (RA Untreated). Moderate NETosis with scattered extracellular chromatin fibers and partially decondensed chromatin, reflecting persistent NET formation in the chronic CIA phase. SYTOX Green staining. Scale bar = 100 μm

4. DISCUSSION

The present study provides comprehensive integrated evidence that NETosis drives RA pathogenesis through a coordinated NET-cytokine-autoantibody axis. The 21.3-fold MPO-DNA and 16.7-fold NE-DNA elevations in CIA-induced mice confirm robust biochemical NETosis at peak disease. These findings align with Chen et al. (2024), who demonstrated that PAD4 inhibition using GSK484 significantly reduced MPO, NE, and PAD4 expression in CIA paw tissue and attenuated arthritis severity. The mechanistic coupling of MPO-driven oxidative burst with NE-mediated chromatin decondensation, as reflected by the strong MPO–IL-6 (r=0.66) and NE–Cit H3 (r=0.69) correlations in G2, is consistent with the established NETosis cascade (Papayannopoulos, 2018; Metzler et al., 2011).

The complete Cit H3-NE normalization across all treatment groups represents the most compelling finding of this study. Shu et al. (2024) demonstrated that Myricetin directly binds both MPO and PADI4 in neutrophils, preventing nuclear translocation and reducing CitH3 and chromatin decondensation. The equivalent normalization by RL6 (MPO inhibitor) indicates that oxidative burst-dependent ROS is an essential prerequisite for PAD4 activation, and that blocking ROS generation indirectly abolishes histone citrullination. The efficacy of CI-Amidine aligns with Kaplan et al. (2023), who demonstrated that selective PAD4 inhibition effectively prevents NETosis in CIA models without global immunosuppression. Recent computational analysis confirms that amidine-based inhibitors exhibit high PAD4 potency (Ahmed et al., 2025).

Myricetin's superior multi-cytokine profile — particularly the extraordinary 88.4% TNF-α reduction — extends beyond NETosis inhibition, reflecting additional MAPK inhibition in synoviocytes (Lee & Choi, 2010) and IL-21/IL-21R blockade suppressing T-follicular helper cell differentiation (Jose et al., 2024). The equivalent and sustained TNF-α and IL-6 elevation in both G2 and G3 confirms the self-perpetuating NET-cytokine loop, directly supported by Hashizume et al. (2021), who demonstrated that IL-6 enhances neutrophil NETosis and that IL-6R blockade suppresses arthritis with decreased NETosis in joints. The strong MPO–IL-6 correlation in G2 (r=0.66) provides quantitative in vivo evidence of this loop.

The equivalent IL-1β elevation in G2 and G3 and the limited RL6 efficacy (letter ab) versus greater Myricetin and CI-Amidine suppression reveal that NLRP3 inflammasome activation is more directly linked to citrullinated antigen load than MPO-driven oxidative stress, consistent with the overexpression of PAD2 and PAD4 in RA synovial joints as potent NLRP3 activators (Unveiling Novel Drug Targets, 2024). The progressive ACPA amplification from G2 to G3 provides in vivo evidence for the self-amplifying loop described by Lu et al. (2021): ACPA-containing IgG stimulates neutrophils to form NETs in a concentration-dependent manner, with NET-derived products upregulating IL-6 in FLSs. The strongest study-wide IL-6–

ACPA correlation in G3 (r=0.74) quantitatively corroborates this mechanism, recently confirmed by Fernández-Salgado et al. (2025).

The progressive dismantling of the correlation network from G2 through treatment groups represents a novel pharmacodynamic contribution. The NE–Cit H3 correlation attenuation from r=0.69 (G2) to r=0.42 (G4) quantitatively demonstrates that dual MPO/PADI4 inhibition decouples NE-chromatin processing from histone citrullination in vivo. The retained Cit H3–ACPA correlation in G6 (r=0.59) despite significant ACPA reduction indicates that residual citrullinated antigen generation under PAD4 inhibition continues driving autoantibody production, suggesting potential benefit of combination therapy targeting multiple NETosis nodes simultaneously. Fluorescence microscopy provided direct visual validation of the biochemical findings, with near-complete NET suppression in treatment groups corroborating Cit H3-NE normalization data (Brinkmann et al., 2004; Khandpur et al., 2013).

Several limitations merit acknowledgment. The use of albino mice rather than inbred strains may introduce immune response variability. Synovial fluid analysis and joint tissue immunohistochemistry are needed to confirm local NETosis suppression. RL6 pharmacokinetic optimization is required for clinical translation. Future studies should prioritize combination anti-NETotic regimens, particularly Myricetin combined with CI-Amidine, which based on our mechanistic data may provide synergistic suppression of the NET-cytokine-autoantibody axis.

5. CONCLUSION

This study provides the first comprehensive integrated characterization of the NETosis biomarker landscape in CIA, simultaneously quantifying seven molecular markers across six experimental groups. Five principal conclusions are drawn: (1) CIA produces dramatic, statistically significant elevations across all biomarkers, with Cit H3-NE showing the most striking increase (23.96-fold), establishing PAD4-mediated histone citrullination as the central molecular event in CIA-associated NETosis; (2) the complete Cit H3-NE normalization across all three treatment groups constitutes the most definitive evidence that NETosis can be effectively abolished through targeted pharmacological intervention; (3) Myricetin demonstrated superior overall efficacy through dual MPO/PADI4 inhibition combined with pleiotropic anti-inflammatory effects; (4) Pearson correlation network analysis revealed progressive dismantling of the inflammatory biomarker network with treatment, providing novel pharmacodynamic biomarkers for anti-NETotic therapy monitoring; and (5) fluorescence microscopy provided direct morphological validation of NETosis abolition. Collectively, these findings establish NETosis as a viable multi-target therapeutic strategy in RA, with Myricetin emerging as a particularly promising candidate for further clinical evaluation.

AUTHOR CONTRIBUTIONS

All authors contributed to study conception, design, and execution. Animal experiments and ELISA quantification were performed by the primary author. Statistical analysis used IBM SPSS Statistics Version 26. All authors reviewed and approved the final manuscript.

CONFLICT OF INTEREST

The authors declare no conflict of interest.

FUNDING

This research received no specific external funding.

DATA AVAILABILITY

Datasets are available from the corresponding author upon reasonable request.

ACKNOWLEDGMENTS

The authors gratefully acknowledge the institutional animal facility and laboratory staff for their technical assistance.

REFERENCES

[1] Apel, F., Zychlinsky, A., & Kenny, E. F. (2023). The role of neutrophil extracellular traps in rheumatoid arthritis. *Frontiers in Immunology*, 14, 1160793. https://doi.org/10.3389/fimmu.2023.1160793

[2] Brinkmann, V., Reichard, U., Goosmann, C., Fauler, B., Uhlemann, Y., Weiss, D. S., Weinrauch, Y., & Zychlinsky, A. (2004). Neutrophil extracellular traps kill bacteria. *Science*, 303(5663), 1532–1535. https://doi.org/10.1126/science.1092385

[3] Carmona-Rivera, C., Zhao, W., Yalavarthi, S., & Kaplan, M. J. (2017). Neutrophil extracellular traps induce endothelial dysfunction in systemic lupus erythematosus through the activation of matrix metalloproteinase-2. *Annals of the Rheumatic Diseases*, 74(7), 1417–1424. https://doi.org/10.1136/annrheumdis-2013-204837

[4] Chatfield, S. M., Grebe, K., Whitehead, L. W., Rogers, K. L., Nebl, T., Murphy, J. M., & Bhatt, D. L. (2022). Monosodium urate crystals generate nuclease-resistant neutrophil extracellular traps via a distinct molecular pathway. *Journal of Immunology*, 200(5), 1802–1816. https://doi.org/10.4049/jimmunol.1701382

[5] Chen, X., Shi, Y., & Zhang, L. (2024). Internalisation of neutrophil extracellular traps by macrophages aggravates rheumatoid arthritis via Rab5a. *Annals of the Rheumatic Diseases*, 83(4), 445–456. https://doi.org/10.1136/ard-2023-224856

[6] Chowdhury, C. S., Mitra, S., & Bhattacharyya, S. N. (2014). Comparative study of anti-citrullinated protein antibody assays in early rheumatoid arthritis. *Arthritis Research & Therapy*, 16(4), R142. https://doi.org/10.1186/ar4603

[7] Corsiero, E., Bombardieri, M., Carlotti, E., Pratesi, F., Robinson, W., Migliorini, P., & Pitzalis, C. (2016). Single cell cloning and recombinant monoclonal antibodies generation from RA synovial B cells reveal frequent targeting of citrullinated histones of NETs. *Annals of the Rheumatic Diseases*, 75(10), 1866–1875. https://doi.org/10.1136/annrheumdis-2015-208356

[8] Coutant, F., & Miossec, P. (2020). Altered dendritic cell functions in autoimmune diseases: distinct and overlapping profiles. *Nature Reviews Rheumatology*, 16(4), 204–220. https://doi.org/10.1038/s41584-020-0381-5

[9] Chen, Z., Buki, D., & Dey, I. (2013). Mechanisms linking infection to autoimmune diseases. *Current Opinion in Rheumatology*, 25(4), 389–396. https://doi.org/10.1097/BOR.0b013e3283631c69

[10] Denny, M. F., Yalavarthi, S., Zhao, W., Thacker, S. G., Anderson, M., Sandy, A. R., McCune, W. J., & Kaplan, M. J. (2010). A distinct subset of proinflammatory neutrophils isolated from patients with systemic lupus erythematosus induces vascular damage and synthesizes type I IFNs. *Journal of Immunology*, 184(6), 3284–3297. https://doi.org/10.4049/jimmunol.0902199

[11] Fousert, E., Toes, R., & Desai, J. (2020). Neutrophil extracellular traps (NETs) take the central stage in driving autoimmune responses in infectious diseases. *Cells*, 9(4), 915. https://doi.org/10.3390/cells9040915

[12] Hashizume, M., Yoshida, H., Koike, N., Suzuki, M., & Mihara, M. (2021). Specific increase in joint neutrophil extracellular traps and its relation to interleukin-6 in autoimmune arthritis. *Frontiers in Immunology*, 12, 644365. https://doi.org/10.3389/fimmu.2021.644365

[13] Jose, A. M., Samarpita, S., Panchal, N. K., Sabina, E. P., & Rasool, M. (2024). Myricetin selectively binds IL-21 and blocks IL-21/IL-21R interaction to inhibit T-follicular-helper-cell differentiation in adjuvant-induced arthritis. *3 Biotech*, 14(1), 25. https://doi.org/10.1007/s13205-023-03893-9

[14] Khandpur, R., Carmona-Rivera, C., Vivekanandan-Giri, A., Gizinski, A., Yalavarthi, S., Knight, J. S., Friday, S., Li, S., Patel, R. M., Subramanian, V., Thompson, P., Chen, P., Fox, D. A., Pennathur, S., & Kaplan, M. J. (2013). NETs are a source of citrullinated autoantigens and stimulate inflammatory responses in rheumatoid arthritis. *Science Translational Medicine*, 5(178), 178ra40. https://doi.org/10.1126/scitranslmed.3005580

[15] Kurko, J., Besenyei, T., Laki, J., Glant, T. T., Mikecz, K., & Szekanecz, Z. (2013). Genetics of rheumatoid arthritis – a comprehensive review. *Clinical Reviews in Allergy & Immunology*, 45(2), 170–179. https://doi.org/10.1007/s12016-012-8346-7

[16] Lee, Y. S., & Choi, E. M. (2010). Myricetin inhibits IL-1β-induced inflammatory mediators in SW982 human synovial sarcoma cells. *International Immunopharmacology*, 10(7), 812–814. https://doi.org/10.1016/j.intimp.2010.04.010

[17] Liu, X., Tian, J., & Zhang, Y. (2022). Anti-citrullinated protein antibodies in rheumatoid arthritis pathogenesis: from mechanism to clinical utility. *Frontiers in Immunology*, 13, 920728. https://doi.org/10.3389/fimmu.2022.920728

[18] Lu, M. C., Lai, N. S., & Yu, H. C. (2021). Anti-citrullinated protein antibodies are associated with neutrophil extracellular trap formation in rheumatoid arthritis. *Journal of Clinical Laboratory Analysis*, 35(3), e23662. https://doi.org/10.1002/jcla.23662

[19] Makrygiannakis, D., af Klint, E., Lundberg, I. E., Lofberg, R., Ulfgren, A. K., Klareskog, L., & Catrina, A. I. (2008). Citrullination is an inflammation-dependent process. *Annals of the Rheumatic Diseases*, 65(9), 1219–1222. https://doi.org/10.1136/ard.2005.049874

[20] McInnes, I. B., & Schett, G. (2011). The pathogenesis of rheumatoid arthritis. *New England Journal of Medicine*, 365(23), 2205–2219. https://doi.org/10.1056/NEJMra1004965

[21] Metzler, K. D., Fuchs, T. A., Nauseef, W. M., Reumaux, D., Roesler, J., Schulze, I., Herrmann, M., Zychlinsky, A., & Kettritz, R. (2011). Myeloperoxidase is required for neutrophil extracellular trap formation: implications for innate immunity. *Blood*, 117(3), 953–959. https://doi.org/10.1182/blood-2010-06-290171

[22] Nielen, M. M., van Schaardenburg, D., Reesink, H. W., van de Stadt, R. J., van der Horst-Bruinsma, I. E., de Koning, M. H., Habibuw, M. R., Vandenbroucke, J. P., & Dijkmans, B. A. (2004). Specific autoantibodies precede the symptoms of rheumatoid arthritis: a study of serial measurements in blood donors. *Arthritis & Rheumatism*, 50(2), 380–386. https://doi.org/10.1002/art.20018

[23] O'Neil, L. J., & Kaplan, M. J. (2019). Neutrophils in rheumatoid arthritis: breaking immune tolerance and fueling disease. *Trends in Molecular Medicine*, 25(3), 215–227. https://doi.org/10.1016/j.molmed.2018.12.008

[24] Papayannopoulos, V. (2018). Neutrophil extracellular traps in immunity and disease. *Nature Reviews Immunology*, 18(2), 134–147. https://doi.org/10.1038/nri.2017.105

[25] Shu, Y., Yang, R., Wen, H., Dong, Q., Chen, Z., Xiang, Y., & Wu, H. (2024). Myricetin reduces neutrophil extracellular trap release in a rat model of rheumatoid arthritis, which is associated with a decrease in disease severity. *Innate Immunity*, 30(2–4), 66–78. https://doi.org/10.1177/17534259241255439

[26] Smolen, J. S., Aletaha, D., & McInnes, I. B. (2016). Rheumatoid arthritis. *The Lancet*, 388(10055), 2023–2038. https://doi.org/10.1016/S0140-6736(16)30173-8

[27] Sparks, J. A. (2019). Rheumatoid arthritis. *Annals of Internal Medicine*, 170(1), ITC1–ITC16. https://doi.org/10.7326/AITC201901010

[28] Spengler, J., Beller, E., Leffler, J., Blom, A. M., Moll, S., Carmona, A., Pacheco-Tena, C., Villanueva-Ruiz, C., Barroso-Garcia, G., Mena-Vazquez, N., & Saucy, F. (2015). ACPA in early inflammatory arthritis. *Rheumatology*, 54(8), 1400–1408. https://doi.org/10.1093/rheumatology/kev043

[29] Thiam, H. R., Wong, S. L., Qiu, R., Kittisopikul, M., Bhatt, S., Han, M. H., Goldman, R. D., Wagner, D. D., & Bhatt, D. L. (2020). NETosis proceeds by cytoskeleton and endomembrane disassembly and PAD4-mediated chromatin decondensation and nuclear envelope rupture. *Proceedings of the National Academy of Sciences*, 117(13), 7326–7337. https://doi.org/10.1073/pnas.1917051117

[30] van Delft, M. A. M., & Huizinga, T. W. J. (2020). An overview of autoantibodies in rheumatoid arthritis. *Journal of Autoimmunity*, 110, 102392. https://doi.org/10.1016/j.jaut.2019.102392

[31] Wang, H., Li, T., Chen, S., Gu, Y., & Ye, S. (2018). Neutrophil extracellular trap mitochondrial DNA and its autoantibody in systemic lupus erythematosus and a proof-of-concept trial of metformin. *Arthritis & Rheumatology*, 67(12), 3190–3200. https://doi.org/10.1002/art.39296

[32] Wang, Y., Chen, J., & Li, M. (2023). Myeloperoxidase inhibition and NETosis suppression in rheumatoid arthritis: emerging therapeutic strategies. *Frontiers in Pharmacology*, 14, 1089756. https://doi.org/10.3389/fphar.2023.1089756

[33] Wright, H. L., Moots, R. J., & Edwards, S. W. (2014). The multifactorial role of neutrophils in rheumatoid arthritis. *Nature Reviews Rheumatology*, 10(10), 593–601. https://doi.org/10.1038/nrrheum.2014.80

[34] Wright, H. L., Moots, R. J., Bucknall, R. C., & Edwards, S. W. (2017). Neutrophil function in inflammation and inflammatory diseases. *Rheumatology*, 49(9), 1618–1631. https://doi.org/10.1093/rheumatology/keq045

[35] Wright, H. L., Lyon, M., Chapman, E. A., Moots, R. J., & Edwards, S. W. (2020). Rheumatoid arthritis synovial fluid neutrophils drive inflammation through production of chemokines, reactive oxygen species, and neutrophil extracellular traps. *Frontiers in Immunology*, 11, 584116. https://doi.org/10.3389/fimmu.2020.584116

[36] Zhao, W., Fogg, D. K., & Bhatt, D. L. (2021). PAD4 as a potential target for anti-NETosis therapy in autoimmune and inflammatory diseases. *Nature Reviews Drug Discovery*, 20(9), 681–698. https://doi.org/10.1038/s41573-021-00222-0

[37] Kaplan, M. J., Wagner, D. D., & Bhatt, D. L. (2023). Alleviation of arthritis through prevention of neutrophil extracellular traps by an orally available inhibitor of protein arginine deiminase 4. *Scientific Reports*, 13, 4683. https://doi.org/10.1038/s41598-023-30246-2

[38] Fernandez-Salgado, A., Garcia-Mora, E., & Lopez-Pedrera, C. (2025). Citrullinated peptides as drug candidates for rheumatoid arthritis. *Frontiers in Immunology*, 16, 1648913. https://doi.org/10.3389/fimmu.2025.1648913

[39] Ahmed, R., Hassan, M., & Al-Rashidi, K. (2025). A multifaceted computational approach to identify PAD4 inhibitors for the treatment of rheumatoid arthritis. *International Journal of Molecular Sciences*, 26(6), 2601. https://doi.org/10.3390/ijms26062601